JOURNAL OF APPLIED ELECTROCHEMISTRY 27 (1997) 93–98

Influence of lead(II) carbonate films of non-antimonial grids on the deep discharge cycling behaviour of maintenance-free lead/acid batteries

R. DE MARCO

School of Applied Chemistry, Curtin University of Technology, GPO Box U 1987, Perth, Western Australia, 6001, Australia

Received 16 November 1995; revised 27 February 1996

The role of hydrocerussite (i.e., $2PbCO_3.Pb(OH)_2$) on the deep discharge cycle-life of non-antimonial lead/acid battery cells was assessed using aged grids comprising deliberately invoked $2PbCO_3.Pb(OH)_2$, and it is shown that, when compared to the untreated grid cells, the aged grid cells required half as many cycles to reach 67% of their initial discharge capacity. The initial specific energy of cells employing aged grids is 40% higher than their untreated grid counterparts; this is attributed to the improved adhesion of the active material to grids containing large amounts of hydrocerussite. A mechanism involving the hydrocerussite-induced formation of a barrier layer in the grid corrosion layer is proposed to explain the premature capacity loss of non-antimonial battery cells.

1. Introduction

It is common practice to employ non-antimonial grids in the manufacture of maintenance-free lead/acid batteries. The removal of antimony from the grid lowers the rate of hydrogen evolution at the negative plate, in turn, reducing the water loss associated with gassing. Today, the emphasis of lead/acid battery research is the development of maintenance-free batteries for a range of applications (e.g., standby power, remote-area power-supply, portable power, electric vehicles etc.). Unfortunately, the poor deep-discharge cycling performance of non-antimonial batteries, which is better known as the antimony-free effect, is an impediment to this research direction.

Although the exact mechanism(s) of the antimony-free effect is unknown, there have been several useful studies of this phenomenon. Pavlov and co-workers [1, 2] have demonstrated that a lead(II) sulfate overlayer on lead will promote the formation of an underlayer of α-PbO at high applied potentials (i.e., $> 900\,mV$ with respect to the $Hg|Hg_2SO_4$ reference electrode). Arifiku *et al.* [3] used ion probe microanalysis to show that antimony is concentrated within the grid corrosion layer at the interface between the metal and the corrosion film, and Hill [4] proposed that the presence of $PbSb_2O_6$ (which is isomorphous with α-PbO_2) at the interface between the grid and the corrosion layer will improve battery cycle-life by strengthening the adhesion of the active material (α-PbO_2) to the corrosion film of the grid.

A number of authors [5–9] have proposed possible causes of the antimony-free effect. Dimitrov and Pavlov [5] claimed that the antimony-free effect is attributable to the formation of a grid passivation layer that restricts the transfer of charge between the active material and the grid corrosion layer. Likewise, Hollenkamp *et al.* [6] detected a low conductivity bilayer corrosion film on non-antimonial grids (i.e., PbO contacting the grid with PbO_2 on top) using electron probe microanalysis. Several workers [7–9] discussed the implications of the active material on the premature capacity loss of non-antimonial lead/acid batteries. Pavlov [7] proposed that gel zones in the active material and the corrosion layer (i.e., hydrated linear chains of PbO_n) are bound together by dopant ions (e.g., antimony) improving the conductivity of the corrosion layer and the active material along with the deep discharge cycle-life of batteries. Alternatively, Winsel *et al.* [8] proposed a three dimensional array of active material comprising neck zones electrically connecting the particles, and the capacity loss of batteries is attributable to shrinkage and/or conversion of the neck zones to the insulator $PbSO_4$. Finally, Dietz *et al.* [9] demonstrated that the premature capacity loss of non-antimonial batteries, at low levels of overcharge, is associated with stratification of the sulfuric acid electrolyte and sulfation of the active material.

Recently, De Marco and Liesegang [10] characterized a range of commercial lead/acid battery grids using the techniques: X-ray photoelectron spectroscopy (XPS); X-ray diffraction (XRD); and metallurgical microscopy. It was shown that the alloy constituents (i.e., Ca, Sn and Sb) segregate to the grid surface during atmospheric oxidation, and this surface enhancement is improved with fine-grained alloys. In addition, it was found that the lead(II) carbonate phase hydrocerussite (i.e., $2PbCO_3.Pb(OH)_2$) formed on non-antimonial grids stored in air, but not on antimonial ones. These authors proposed that, in the early stages of a battery's life (i.e., curing,

0021-891X

forming and the initial period of charge/discharge cycling), the $2PbCO_3.Pb(OH)_2$ film of non-antimonial grids induces the formation of an underlayer deposit of α-PbO in the grid corrosion film; this is due to the hydrocerussite overlayer providing the alkaline conditions (i.e., $pH > 13$) needed for the thermodynamic stabilization of α-PbO. Finally, De Marco and Liesegang [10] suggested that the antimony-free effect might be alleviated by carrying out deliberate oxidation of grids to encourage the oxidation-induced surface segregation of Sn which is beneficial to deep-discharge cycle-life [11]. This must be performed in a CO_2-free atmosphere (e.g., artificial air comprising high-purity oxygen and nitrogen) to prevent the formation of detrimental $2PbCO_3.Pb(OH)_2$.

Despite the complex nature of the mechanism of the antimony-free effect, the findings of the research into this phenomenon suggest that it is caused by a reduction in the conductivity of both the grid corrosion layer and the active material. Nevertheless, it is generally believed that the α-PbO barrier layer mechanism is the likely explanation of the antimony-free effect, as the presence of a passivation film around the grid would restrict significantly the transfer of charge between the active material (i.e., PbO_2) and the current collecting grid, causing the usual rapid capacity loss.

Although the antimony-free effect has been studied in detail [1–11], there has been no attempt to investigate the role of grid hydrocerussite on the deep discharge cycling behaviour of non-antimonial lead/acid batteries. The aim of this study was to ascertain the effect of grid hydrocerussite on the cycle-life of 2 V maintenance-free lead/acid battery cells. It was deemed necessary to employ a cycling regime that accelerated the rate of capacity loss in order to exemplify and clearly establish the effect(s) of grid hydrocerussite.

2. Experimental details

2.1. *Ageing of grids*

Previous work by the author [10] has shown that ageing of lead–calcium–tin grids in humidified conditions for four weeks promotes the formation of copious quantities of the lead(II) carbonate phase hydrocerussite (i.e., $2PbCO_3.Pb(OH)_2$). Six lead–calcium–tin grids were placed on a glass stand above a small pool of water in a sealed polyethylene container, and aged in an oven at 50°C for eight weeks. A longer ageing period was employed in this study to promote the formation of a thicker hydrocerussite film around the grids.

2.2. *Preparation of pasted plates*

Positive plates were prepared using the paste formula given in Table 1 [12]. Barton-pot leady oxide obtained from the New South Wales plant of GNB Battery Technologies and Analytical Reagent Grade sulfuric acid (BDH, AnalaR) were used in the preparation of the paste. The paste mixing procedure entailed the addition of five separate 50 mL quantities of ultrahigh purity water to the nominal quantity of dry ingredients (i.e., leady oxide, fibre and carboxymethyl cellulose) with mixing for 2 min after each addition. Acid was then added to the mixture (four separate additions of 33 mL), and the paste was mixed for 2 min after each addition. Finally, the remainder of the water was added to the paste, and its density was recorded after 2 min of mixing by measuring the volume of water displaced by 100 g of paste. The paste was then applied by hand to lead–calcium–tin grids that are commonly used in the manufacture of GNB Powersafe batteries. Previous grid analysis using inductively-coupled plasma atomic emission spectrometric analysis revealed that they contained 0.1 wt% Ca and 0.4 wt% Sn [10].

Table 1. Paste formula for preparation of positive plates

Component	*Positive paste*
Leady oxide/kg	2
Fibre/g	0.6
Carboxymethyl cellulose/g	5
1.40 rel. density H_2SO_4/mL	132
Water/mL	300
Acid-to-oxide ratio/wt%	4.7
Paste density/g mL^{-1}	4.6–4.7

The pasted plates were cured under 50°C high humidity conditions in a sealed polyethylene container for 24 h, followed by drying at 50°C for a further 24 h period. The individual plates were placed in intimate contact with surrounding plates in order to mimic the curing conditions commonly employed in battery production [13].

2.3. *Assembly of 2 V cells*

The dried plates were assembled into 2 V cells comprising one positive plate surrounded by two negative plates. The cured negative plates were produced in the factory of GNB Battery Technologies using a paste recipe and curing conditions similar to those described elsewhere by Manders *et al.* [12]. Note that the alloy composition of GNB negative grids is identical to that of their positives. The positive and negative plates were separated from each other using only absorptive glass-fibre separators (~3 mm thick) manufactured by GNB Battery Technologies, and the cells were placed in GNB Powersafe battery containers. The plates were formed in 1.2 L of 1.07 relative density H_2SO_4 using a constant current of 5 A for 6 h, and then rested at open circuit for 1 h to allow the sulfuric acid depleted diffusion layers of the pores to be replenished by the permeation of fresh electrolyte. The charge/rest period was repeated, followed by a final charge at 5 A for 6 h. After formation, the sulfuric acid and separators were discarded, and the cells were reassembled and filled with 1.3 L of 1.270 relative density H_2SO_4.

Note that in all cases the electrolyte-to-positive plate material ratio of the cells was 4.3 mL per g.

2.4. *Cycle-life evaluation of cells*

The cycle-life performance of 2 V cells was assessed by employing a Digatron BTS-500 computerized charge/discharge unit (Digatron GmbH, Germany) to undertake repetitive charge/discharge cycling at the 3 h rate. After charging to 2.55 V at 5.6 A, the cells were held at the top-of-charge voltage until the current had tapered to 1 A. At this juncture, the cells were discharged at 5.6 A until a voltage of 1.75 V was reached. The charge/discharge procedure was repeated until the discharge capacity fell to 50% of its original value.

2.5. *Autopsies of cells*

The failed cells were dismantled, and the positive plates were rinsed in distilled water followed by drying at 50 °C for 24 h. The wet positive plates and glass separators were inspected manually to ascertain if active material shedding was a significant cause of cell failure. Finally, the approximate resistances of dry plates at various locations were measured using a multimeter. At each location, the surface of the active material was pierced by the probes to provide a resistance that was representative of the sampled location.

3. Results and discussion

3.1. *Cycling of cells*

Preliminary work undertaken using the two-step constant current (CC) charging regime of Hollenkamp *et al.* [6] (i.e., an initial current of 5.6 A up to 2.55 V followed by 1 A until a charge-to-discharge ratio (i.e., C/D) of 1.2 was reached) had shown that the rate of decline in discharge capacity of untreated grid cells was very slow over the first six cycles (i.e., 0.7 Ah kg^{-1} of cured material per cycle) and, beyond this point, it rose and eventually overtook the initial discharge capacity after approximately 17 cycles. This behaviour was partly attributed to the fact that the second step of the two-step CC charging process at 1 A to a C/D of 1.2 was achieved through the cell potential floating up to 2.8–2.9 V. Under these conditions of high overpotential, the charging reactions (i.e., PbO_2 and Pb formation) are driven closer to completion. In addition, the charge/discharge data for the two-step CC charging process revealed that the charge acceptance of the cells at the lower and more efficient charging rate of 1 A increased gradually as the cells were cycled. These factors combined to increase the discharge capacity on cycling with the two-step CC charging regime. Alternatively, the rate of discharge capacity loss was accelerated and a cessation in decline was avoided by using the cycling regime described in Section 2.4 because the charging reactions did not proceed to the same extent under the conditions of lower overpotential associated with restriction of the top-of-charge voltage to 2.55 V, and there was no trickle charging at 1 A.

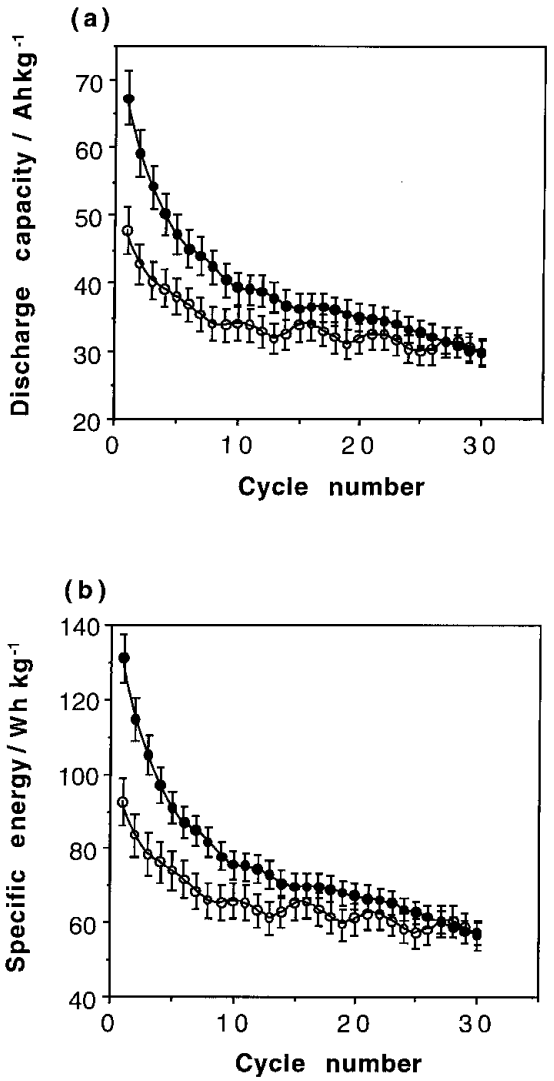

Fig. 1. Discharge data for cells prepared using (o) untreated and (•) humidified grids. Discharge capacity data are presented in (a), and results for specific energy are given in (b).

Figure 1(a) and (b) show discharge capacity (Ah kg^{-1}) and specific energy (Wh kg^{-1}) data (averaged over six grids of each type) for 2 V cells prepared using (o) untreated and (•) humidified grids, respectively. It can be seen that the initial discharge capacity and specific energy of humidified grid cells are 1.4 times higher than those of the untreated grids. The strength of adhesion of the cured material to the grid was estimated by measuring the weight loss after dropping plates from a height of 3 m (refer to Table 2

Table 2. Weight losses (expressed as a percentage of total cured material weight) after drop testing of cured plates from a height of 3 m

Grid type	*Weight loss /%*
Untreated	11.2±3
Humidified	3.4±1.7

for data averaged over three grids of each type). This test assumes that the cohesive strength (i.e., the inter-particle forces holding the cured material together) is the same in each type of plate (fabricated using the same paste recipe) and any deviation in weight loss is attributable to a variation in the adhesive strength. Clearly, the results suggest that the enhancement in specific energy is linked to an improvement in the adhesion of the cured material to the humidified grid surface. It is important to note that previous XRD work [10] has detected hydrocerussite diffraction peaks for humidified grids demonstrating that the hydrocerussite film is crystalline and relatively thick. Presumably, the tribasic lead sulfate phase of cured material is capable of networking with the thick crust of hydrocerussite, and this improves the adhesion of the cured material to the grid. This argument is supported by the patent of the General Motors Corporation [14] which stipulates that surface oxidation of lead grids improves the adhesion of cured material to the grid.

The characteristic premature capacity loss of the non-antimonial cells (refer to Fig. 1), which is dubbed the antimony-free effect, is clearly evident in the initial 10 cycles, and the rate of decline in discharge capacity for the untreated cells of about 1.5 Ah kg^{-1} per cycle is similar to that reported recently by Hollenkamp *et al.* [6] with non-antimonial batteries at a low level of overcharge (i.e., C/D of 1.1). By contrast, the cells employing humidified grids displayed a faster rate of diminution in discharge capacity of approximately 3 Ah kg^{-1} per cycle. Additional cycling data to 60 cycles (not shown) followed the same gradual decline in discharge capacity as noted over 10–30 cycles. Although the rate of capacity loss over 30–60 cycles was marginally higher for humidified grid cells over untreated ones, the very slow rate of decline (i.e., 0.26–0.32 Ah kg^{-1} per cycle) was similar to that noted with high durability antimonial batteries [6]. Clearly, the hydrocerussite film of humidified grids invokes a memory effect that only pertains to the early stage of cycling (i.e., 1–30 cycles). Consequently, the charge/discharge data was only reported over this cycling period.

The difference in the rate of decline in discharge capacity is exemplified by the active-material utilization (i.e., measured discharge capacity over the corresponding theoretical capacity) and percentage initial discharge capacity data presented in Fig. 2(a) and (b), respectively. It can be seen that the initial active-material utilization of cells (calculated by assuming all Pb is present as $3PbO.PbSO_4.H_2O$ in the cured material) has been estimated at 23% and 32% in the untreated and humidified grid cells, respectively. Note that these values are similar to the one deduced by Hollenkamp *et al.* [6] for non-antimonial batteries using the XRD composition of discharged positive active material. The variation in initial active-material utilization of the two types of cell is attributable to the improved adhesion of the active material to the humidified grid surface (refer to

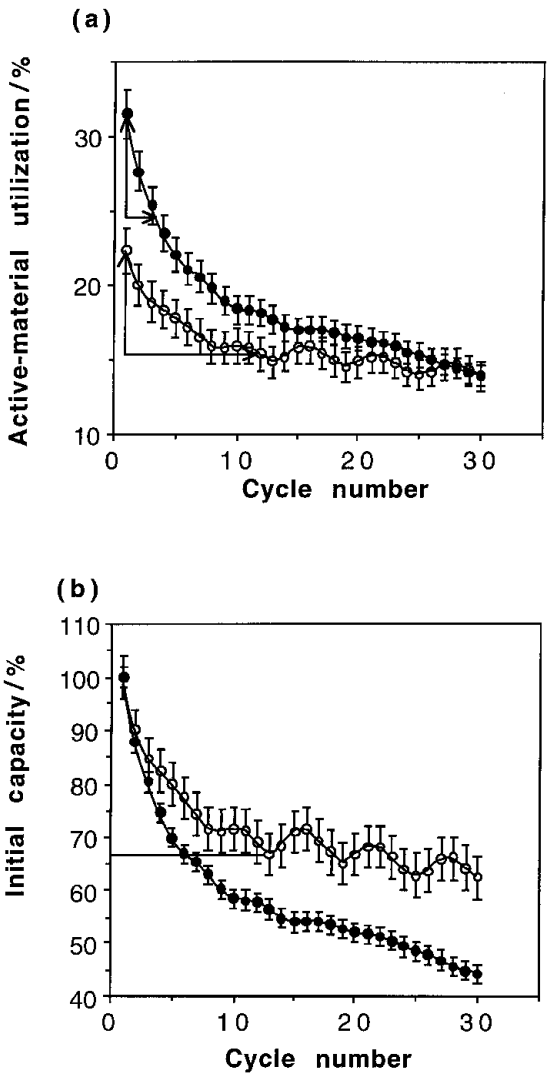

Fig. 2. Cycling data as a function of cycle number for cells prepared using (o) untreated grids and (•) humidified grids: (a) active-material utilization; (b) percentage initial discharge capacity.

Table 2). Figure 2(a) clearly shows a 6.5% loss of active-material utilization (i.e., a loss of 6.5% of total available active material) occurs over three cycles with humidified grids, while the untreated grid cells lose the same level of active-material utilization after 12 cycles (refer to the marked regions of Fig 2(a)). An alternative perspective is the discharge capacity of cells employing humidified grids reaches 67% of its initial value after six cycles, while the untreated grid cells achieve this condition after 13 cycles.

It is proposed that the premature capacity loss of non-antimonial grid cells is facilitated by the hydrocerussite film of the grids. Presumably, this is due to the barrier layer mechanisms proposed by De Marco and Liesegang [10] and Pavlov [15]. With this mechanism, the $2PbCO_3.Pb(OH)_2$ species intimately contacts the grid and active material and, as the grid oxidizes during pasting and curing, a barrier layer of α-PbO is formed at the surface of the grid. In addition, the grid surface film of hydrocerussite in non-antimonial cured plates will cause a memory effect during formation and cycling as the metasomatic processes of

grid corrosion result in the formation of PbO_2 agglomerates that are similar in size and shape to the large $2PbCO_3.Pb(OH)_2$ crystals of humidified grids (XRD detected intense and narrow hydrocerussite diffraction peaks signifying the presence of large crystallites [10]). Significantly, the conversion of these large crystallites into big PbO_2 agglomerates will reduce both the surface area and conductivity of the grid/active material interface causing a loss in discharge capacity [15].

The cumulative specific energy of 2 V cells was calculated by summing the specific energies of all cycles prior to and including the point at 67% of initial discharge capacity shown in Fig. 2(b). This parameter is taken as a reliable indicator of battery performance as it reflects the amount of work that can be done by a battery in a specified window of discharge capacity (i.e, 100–67%) [12]. The results (933 and 626 $Wh\,kg^{-1}$ for untreated and humidified grids, respectively) demonstrate that the faster rate of degradation for the cells employing humidified grids had lowered considerably the energy output (i.e., by 33%) despite the boost in initial specific energy noted in Fig. 1.

3.2. *Charging and capacity loss*

Another important trend was gleaned from the cycling data of Fig. 2(a). It can be seen that the rate of decline in active-material utilization for both the untreated and aged grid cells was rapid during the first 10 cycles (i.e., 0.6–1.3% per cycle) while a much lower rate of diminution is obtained between 10 and 30 cycles (i.e., 0.1–0.2% per cycle). Presumably, a different mechanism of premature capacity loss is responsible for this disparate behaviour. Note that the discrepancy between C/D values of the two cell types in cycle 1 might be due to a contact resistance at the grid/active material interface leading to an ohmic overpotential for untreated cells where the adhesion of cured material to the grid is inferior to that of humidified grids. In any event, an examination of the C/D values of both types of cells (refer to Fig. 3) demonstrates that the faster rate of decline in discharge capacity is associated with high values of C/D (i.e., $C/D > 1$), while the slower rate of diminution occurs at low values of C/D (i.e., $0.95 < C/D > 1.05$).

Hollenkamp *et al.* [6] have shown that the rate of premature capacity loss of non-antimonial cells is affected by the C/D, i.e., faster rates of decline are obtained at higher values of C/D. For a reversible electrochemical system such as the lead/acid battery, it is likely that the rapid grid corrosion caused by the overcharge noted in this study results in the formation of a passivation layer of α-PbO at the active material/grid corrosion layer interface, and this reduces both the exchange of electrons and the discharge capacity in the discharge step of the cycle. Note that water decomposition starts at 2.4 V and

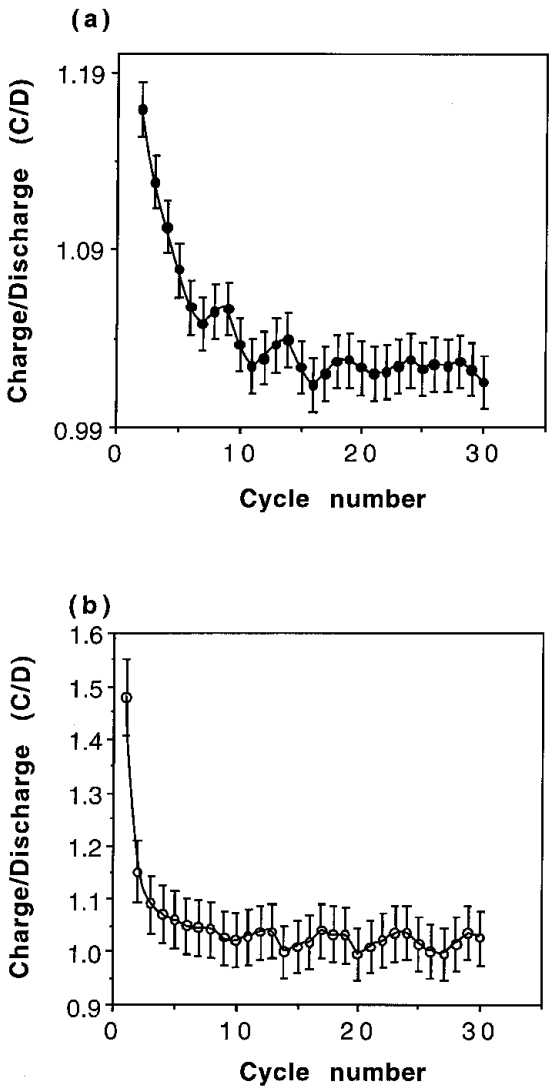

Fig. 3. Charge/discharge ratios (C/D) as a function of cycle number for cells prepared using (•) humidified and (o) untreated grids.

restriction of the top-of-charge voltage to 2.55 V ensured that the rates of hydrogen and oxygen evolution were very slow. Under these conditions, it is expected that only a very small quantity of water will be decomposed over the initial 30 cycles (consisting of about 25 cycles at low C/D values of 1–1.05) and, in fact, the cells did not lose any water throughout the cycling tests. On the other hand, the lower C/D values in the latter portion of cycling indicate a lower rate of grid corrosion and demise in discharge capacity.

The origin of the diminution in C/D during cycling is not known; however, it is possible that the growth of the corrosion layer involves the conversion of outer PbO to PbO_2 while additional PbO forms at the grid/corrosion layer interface as the grid continues to corrode. This scenario, which is consistent with the observation of Hollenkamp *et al.* [6] of a bilayer corrosion film on non-antimonial grids, would improve the conductivity of the grid corrosion layer in the later stages of cycling (i.e. > 10 cycles).

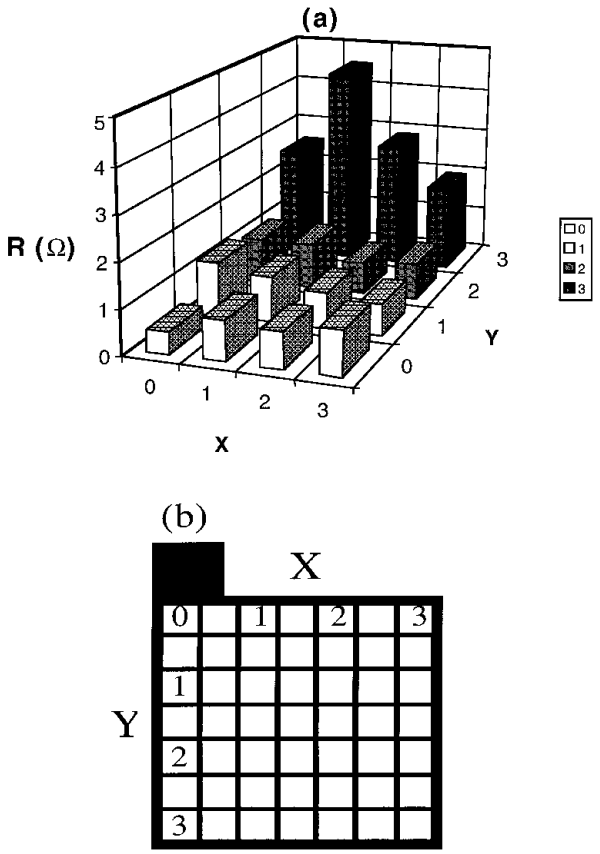

Fig. 4. The electrical resistance profile of a positive plate (width 18 cm × height 14 cm) at the end of cycling (a), and (b) shows the locations at which the resistances were measured.

3.3. *Autopsies of failed cells*

Finally, autopsies of failed cells revealed that active material shedding was not responsible for their demise. In all cases, the active material was intact and very little had broken away from the plates. As suggested previously [9], the spatial variation in plate resistances (i.e., low-to-high resistance from top-to-bottom) for a rinsed and dry plate at the locations shown in Figure 4(b) (refer to Fig. 4(a) for resistances) indicate that stratification of the electrolyte and sulfation of the active material is another factor leading to the failure of the cells. It is important to note that, at a discharge current of 5.6 A, the high ohmic potential of active material with a resistance of 1–5Ω (i.e., 5.6–28 V) is both unrealistic and unobtainable. This apparent anomaly must be due to the high contact resistances of PbO_2 particles in the dry and porous positive active material (PAM), while a conductive pathway exists between the particles when the pores of the PAM are occupied by the sulfuric acid electrolyte.

4. Conclusion

Charge/discharge cycling of 2 V cells prepared using humidified non-antimonial grids has demonstrated that the hydrocerussite film of such grids increases the rate of decline in discharge capacity under deep-discharge duty. This observation is consistent with the barrier layer mechanism of De Marco and Liesegang [10] and Pavlov [15] involving the hydrocerussite-induced passivation of the grid corrosion layer of non-antimonial batteries. Grid surface hydrocerussite is the likely cause of the antimony-free effect.

Autopsies of the failed non-antimonial cells have indicated that sulfation of the active material is another cause of premature capacity loss. Although the cycling data reveal that sulfation of active material is one cause of premature capacity loss, the results of this study demonstrate that the surface chemistry of non-antimonial grids is a major factor in the mechanism of the antimony-free effect. Presumably, this is related to the corrosion chemistry of non-antimonial grids which might involve the formation of a barrier layer of α-PbO [5, 6, 10, 11] and/or a low surface area/low conductivity corrosion layer [15].

Future work will entail a study of the active material and grid corrosion layers at different stages of cycling using XRD and microscopic techniques. This will allow a deduction of the mechanisms pertaining to capacity loss of non-antimonial cells subjected to different cycling conditions.

Acknowledgements

The author thanks GNB Battery Technologies for providing the battery materials used in this study, and the Australian Research Council for financial assistance.

References

[1] D. Pavlov, C.N. Poulieff, E. Klaja and N. Iordanov, *J. Electrochem. Soc.*, **116** (1969) 316.
[2] D. Pavlov and N. Iordanov, *ibid.* **117** (1970) 1103.
[3] F. Arifuku, H. Yoneyama and H. Tamura, *J. Appl. Electrochem.* **9** (1979) 629.
[4] R.J.Hill, *J.Solid State Chem.* **7** (1987) 12.
[5] M.K. Dimitrov and D. Pavlov, *J. Power Sources* **46** (1993) 203.
[6] A.F. Hollenkamp, K.K. Constanti, M.J. Koop, L. Apateanu, M. Calabek and K. Micka, *ibid.* **48** (1994) 195.
[7] D. Pavlov, *ibid.* **48** (1994) 179.
[8] A. Winsel, E. Voss and U. Hullmeine, *ibid.* **30** (1990) 209.
[9] H. Dietz, H. Niepraschk, K. Wiesener, J. Garche and J. Bauer, *ibid.* **46** (1993) 191.
[10] R. De Marco and J. Liesegang, *Appl. Surf. Sci.* **84** (1995) 237.
[11] A.F. Hollenkamp, *J. Power Sources* **36** (1991) 567.
[12] J.E. Manders, L.T. Lam, R. De Marco, J.D. Douglas, R. Pillig and D.A.J. Rand, *ibid.* **48** (1994) 113.
[13] H. Ozgun, L.T. Lam, D.A.J. Rand and S.K. Bhargava, *ibid.* **52** (1994) 159.
[14] General Motors Corporation, US Patent 3867200 (1975).
[15] D. Pavlov, *J. Power Sources* **53** (1995) 9.